Search for three-nucleon force effects on the longitudinal response function of ^{4}He

Sonia Bacca,[1,*] Nir Barnea,[2,†] Winfried Leidemann,[3,‡] and Giuseppina Orlandini[3,§]
[1]*TRIUMF, 4004 Wesbrook Mall, Vancouver, British Columbia, V6J 2A3, Canada*
[2]*Racah Institute of Physics, Hebrew University, 91904 Jerusalem, Israel*
[3]*Dipartimento di Fisica, Università di Trento, and INFN (Gruppo Collegato di Trento), via Sommarive 14, I-38100 Trento, Italy*
(Received 25 September 2009; published 3 December 2009)

A detailed study of the ^{4}He longitudinal response function $R_L(\omega, q)$ is performed at different kinematics, with particular emphasis on the role of three-nucleon forces. The effects reported are the results of an *ab initio* calculation where the full four-body continuum dynamics is considered via the Lorentz integral transform method. The contributions of the various multipoles to the longitudinal response function are analyzed, and integral properties of the response are discussed as well. The Argonne V18 nucleon-nucleon interaction and two three-nucleon force models (Urbana IX and Tucson-Melbourne′) are used. At lower momentum transfers ($q \leqslant 200$ MeV/c) three-nucleon forces play an important role. One even finds a dependence of R_L on the three-nucleon force model itself, with differences of up to 10%. Thus a Rosenbluth separation of the inclusive electron scattering cross section of ^{4}He at low momentum transfers would be of great value for differentiating among force models.

DOI: 10.1103/PhysRevC.80.064001 PACS number(s): 25.30.Fj, 21.45.−v, 27.10.+h, 31.15.xj

I. INTRODUCTION

An aspect of nuclear dynamics that has attracted a lot of interest in recent years is the importance of multinucleon forces and, in particular, of the three-nucleon force (3NF). The nuclear potential clearly has an *effective* nature; therefore it is, in principle, a many-body operator. However, for several decades the debate has concentrated mainly on its two-nucleon part. This debate has taken place among the advocates of three different approaches based on: meson theory, pure phenomenology, and, more recently, effective field theory. Realistic potentials have been obtained within the three frameworks, relying on fits to thousands of N-N scattering data. It is well known that such realistic potentials do not explain the triton binding energy and thus 3NFs are necessary. Today, because of effective field theory approaches, a new debate is taking place regarding the 3NF. However, for the determination of a *realistic* three-body potential or the discrimination among different models one needs to find $A \geqslant 3$ observables that are 3NF sensitive. Significant effort in this direction has taken place in recent years, with accurate calculations of bound-state properties of nuclei of increasing mass number A [1,2].

We follow a complementary approach and direct our attention, instead, toward electromagnetic reactions in the continuum. In fact many years of electron scattering experiments have demonstrated the power of electronuclear reactions, in particular, of inelastic ones, to provide important information on nuclear dynamics. The possibility to vary the energy ω and momentum q transferred by the electron to the nucleus allows one to focus on different dynamic aspects. In fact one might find regions where the searched three-nucleon effects are sizable. The choice of the ^{4}He target is particularly appropriate because of the following considerations. (i) The ratio of the number of triplets to the number of pairs goes as $(A-2)/3$, and therefore is doubling from ^{3}He to ^{4}He. (ii) Theoretical results on hadronic scattering observables involving four nucleons have already shown that three-body effects are rather large [3,4]. (iii) Because ^{4}He has quite a high average density and its binding energy per particle is similar to that of heavier systems, it can serve as a guideline to investigate heavier nuclei. (iv) Various *inclusive* ^{4}He (e, e') experiments have been performed in the past [5], in which Rosenbluth separations have been carried out. Because of the low atomic number it is possible to study longitudinal and transverse responses separately, without the ambiguities created by the Coulomb distortions affecting heavier systems. (v) The Lorentz integral transform (LIT) method [6,7] allows extension of investigations beyond the three- and four-body breakup thresholds.

In this work we concentrate on the longitudinal response function $R_L(\omega, q)$ at constant momentum transfers $q \leqslant 500$ MeV/c. Because the longitudinal response R_L is much less sensitive to meson exchange effects than the transverse response R_T, the use of a simple one-body density operator allows us to concentrate on the nuclear dynamics generated by the potential. In fact, for low q, two-body operators in R_L are only of fourth order in effective field theory counting (at next-to-next-to-next-to leading order, N^{3}LO) [8], and their contribution is negligible up to $q \approx 300$ MeV/c; see Sec. V.

Besides presenting new results, this work gives a more detailed analysis of those published in a previous Letter [9]. The paper is organized as follows. In Sec. II we give the definition of R_L and explain the theoretical framework that allows its calculation. In Sec. III we present the results for different kinematics and compare our results with existing data. In Sec. IV we analyze our results as obtained from a multipole decomposition of the response function. In Sec. V we discuss integral properties of the longitudinal response and

*bacca@triumf.ca
†nir@phys.huji.ac.il
‡leideman@science.unitn.it
§orlandin@science.unitn.it

compare them with some of the results in the literature. Finally, conclusions are drawn in Sec. VI.

II. THEORETICAL FRAMEWORK

In the one-photon-exchange approximation, the inclusive cross section for electron scattering off a nucleus is given in terms of two response functions, that is,

$$\frac{d^2\sigma}{d\Omega d\omega} = \sigma_M \left[\frac{Q^4}{q^4} R_L(\omega, q) + \left(\frac{Q^2}{2q^2} + \tan^2\frac{\theta}{2}\right) R_T(\omega, q)\right], \tag{1}$$

where σ_M denotes the Mott cross section; $Q^2 = -q_\mu^2 = q^2 - \omega^2$, the squared four-momentum transfer with ω and $\mathbf{q}$ the energy and three-momentum transfers, respectively; and θ is the electron scattering angle. The longitudinal and transverse response functions $R_L(\omega, q)$ and $R_T(\omega, q)$ are determined by the transition matrix elements of the Fourier transforms of the charge and the transverse current density operators. In this work we focus on the longitudinal response, which is given by

$$R_L(\omega, q) = \sum\!\!\!\!\!\!\int_f |\langle \Psi_f | \hat{\rho}(\mathbf{q}) | \Psi_0 \rangle|^2 \delta\left(E_f + \frac{q^2}{2M} - E_0 - \omega\right), \tag{2}$$

where M is the target mass and $|\Psi_{0/f}\rangle$ and $E_{0/f}$ denote initial- and final-state wave functions and energies, respectively. The charge density operator ρ is defined as

$$\hat{\rho}(\mathbf{q}) = \frac{e}{2} \sum_k \left(1 + \tau_k^3\right) \exp\left[i\mathbf{q}\cdot\mathbf{r}_k\right], \tag{3}$$

where e is the proton charge and τ_k^3 is the isospin third component of nucleon k. The δ function ensures energy conservation.

As will become clear in Sec. III it is useful to consider the charge density operator as being decomposed into isoscalar (S) and isovector (V) contributions:

$$\begin{aligned}\hat{\rho}(\mathbf{q}) &= \frac{e}{2} \sum_k \exp\left[i\mathbf{q}\cdot\mathbf{r}_k\right] + \frac{e}{2} \sum_k \tau_k^3 \exp\left[i\mathbf{q}\cdot\mathbf{r}_k\right] \\ &\equiv \hat{\rho}_S(\mathbf{q}) + \hat{\rho}_V(\mathbf{q}).\end{aligned} \tag{4}$$

Each of them can be further decomposed into Coulomb multipoles [10],

$$\hat{\rho}_X(\mathbf{q}) = 4\pi \sum_{J\mu} \hat{C}_\mu^{J,X}(q)\, Y_\mu^J(\hat{q})^*, \tag{5}$$

where the Coulomb multipole operators $\hat{C}_\mu^{J,X}(q)$ are defined by

$$\hat{C}_\mu^{J,X}(q) \equiv \frac{1}{4\pi} \int d\hat{q}'\, \hat{\rho}_X(\mathbf{q}') Y_\mu^J(\hat{q}'), \tag{6}$$

with $X = S, V$ and $Y_\mu^J(\hat{q})$ denotes the spherical harmonics.

From Eq. (2) it is evident that, in principle, knowledge of all possible final states excited by the electromagnetic probe, including, of course, states in the continuum, is required. Thus, in a straightforward evaluation both bound and continuum states would have to be calculated. The latter constitute the major obstacle for a many-body system, as complete many-body scattering wave functions are not yet accessible for $A > 3$. In the LIT method [6,7] this difficulty is circumvented by considering, instead of $R_L(\omega, q)$, the integral transform $\mathcal{L}_L(\sigma, q)$ with a Lorentzian kernel defined for a complex parameter $\sigma = \sigma_R + i\,\sigma_I$ by

$$\mathcal{L}_L(\sigma, q) = \int d\omega \frac{R_L(\omega, q)}{(\omega - \sigma_R)^2 + \sigma_I^2} = \langle \widetilde{\Psi}_{\sigma,q}^\rho | \widetilde{\Psi}_{\sigma,q}^\rho \rangle. \tag{7}$$

The parameter σ_I determines the resolution of the transform and is kept at a constant finite value ($\sigma_I \neq 0$). The basic idea of considering $\mathcal{L}_L$ lies in the fact that it can be evaluated from the norm of a function $\widetilde{\Psi}_{\sigma,q}^\rho$, which is the unique solution of the inhomogeneous equation

$$(\hat{H} - E_0 - \sigma) | \widetilde{\Psi}_{\sigma,q}^\rho \rangle = \hat{\rho}(q) | \Psi_0 \rangle. \tag{8}$$

Here $\hat{H}$ denotes the nuclear Hamiltonian. The existence of the integral in Eq. (7) implies that $\widetilde{\Psi}_{\sigma,q}^\rho$ has asymptotic boundary conditions similar to those of a bound state. Thus, bound-state techniques can be applied for its solution. Here we use the effective interaction hyperspherical harmonics (EIHH) method [11–13].

The response function $R_L(\omega, q = \text{const})$ is then obtained by inverting the integral transform (7). For the inversion of the LIT, various methods have been devised [14,15]. In particular, the issue of the inversion of the LIT is discussed extensively in Ref. [16].

Finally, we should mention that the expression of the charge density in Eq. (3) describes point particles. To compare our results with experimental data, after inversion the isoscalar and isovector parts of R_L have to be multiplied by the proper nucleon form factors,

$$\tfrac{1}{2}\left(1 + \tau_k^3\right) \to G_E^S(Q^2) + \tau_k^3 G_E^V(Q^2), \tag{9}$$

where G_E^S and G_E^V are the isoscalar and isovector form factors:

$$G_E^S = \tfrac{1}{2}\left(G_E^p + G_E^n\right), \tag{10}$$

$$G_E^V = \tfrac{1}{2}\left(G_E^p - G_E^n\right). \tag{11}$$

For on-shell particles, these form factors depend on the squared four-momentum transfer Q^2 alone. In principle, this is no longer true for the off-shell situation. However, in view of the fact that little is known about the off-shell continuation and, furthermore, for the moderate energy and momentum transfers considered in this work, neglecting such effects is justified. Therefore the results reported in Sec. III all include the proton electric form factor with the usual dipole parametrization

$$G_E^p(Q^2) = G_D(Q^2) = \frac{1}{\left(1 + \frac{Q^2}{\Lambda}\right)^2} \tag{12}$$

($\Lambda = 18.43\ \text{fm}^{-2}$). For the neutron electric form factor we use the parametrization from Ref. [17],

$$G_E^n(Q^2) = -\frac{\mu_n \frac{Q^2}{4m^2}}{1 + 5.6\frac{Q^2}{4m^2}} G_E^p(Q^2), \tag{13}$$

with $\mu_n = -1.911829\mu_N$ and m being the nucleon mass.

III. RESULTS OF THE LORENTZ INTEGRAL TRANSFORM CALCULATION

In this section we present results on R_L, focusing on the evolution of dynamic effects as the momentum transfer decreases. Figure 1 shows R_L at constant $q = 200$ and $100\,\mathrm{MeV}/c$, calculated with the Argonne V18 (AV18) potential [19], with the AV18 augmented by the Urbana IX (UIX) [20] 3NF, and with the Malfliet-Tjon (MT) potential [21]. As shown in Ref. [9] there is a large quenching effect owing to the 3NF, which is strongest at lower q. Note that this effect is not simply correlated with the underbinding of the AV18 potential (binding energy $E_B = 24.35$ MeV in the present LIT calculation; with higher EIHH precision, $E_B = 24.27$ MeV [22]). In fact, if this were the case, the results with the MT potential, which gives a slight overbinding of ^{4}He ($E_B = 30.56$ MeV), would lie even below those obtained with the AV18 + UIX ($E_B = 28.40$ MeV). In contrast, the MT curve is situated between the curve with and the curve without the 3NF.

We do not give results for the threshold region, where there is a 0^+ resonance [23]. In our present calculations we are not able to resolve this narrow resonance; therefore we subtract its contribution before inversion as we do for the elastic peak [7]. This procedure of course does not affect the results above the resonance.

Given the large 3NF effect at lower q it is of interest to determine whether there is a dependence of the results on the 3NF model itself. To this end we also performed the calculation

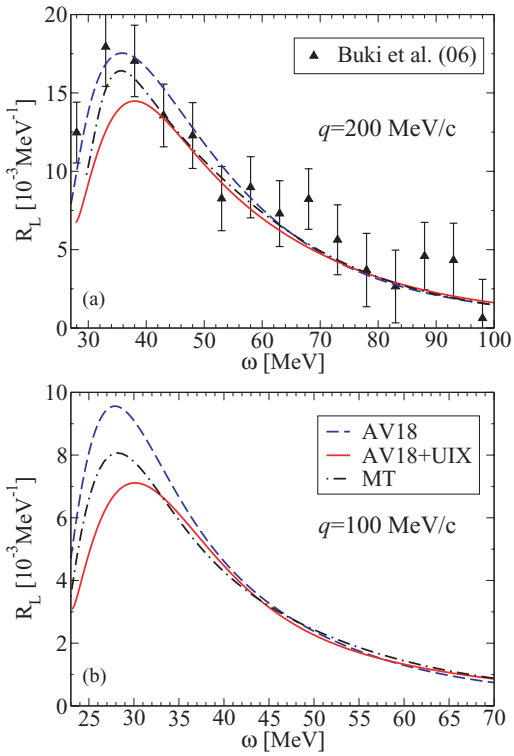

FIG. 1. (Color online) Longitudinal response function for $q = 200$ and $100\,\mathrm{MeV}/c$ with the AV18 (dashed line), AV18 + UIX (solid line), and MT (dashed-dotted line) potentials. Data at $q \simeq 200\,\mathrm{MeV}/c$ are from Ref. [18].

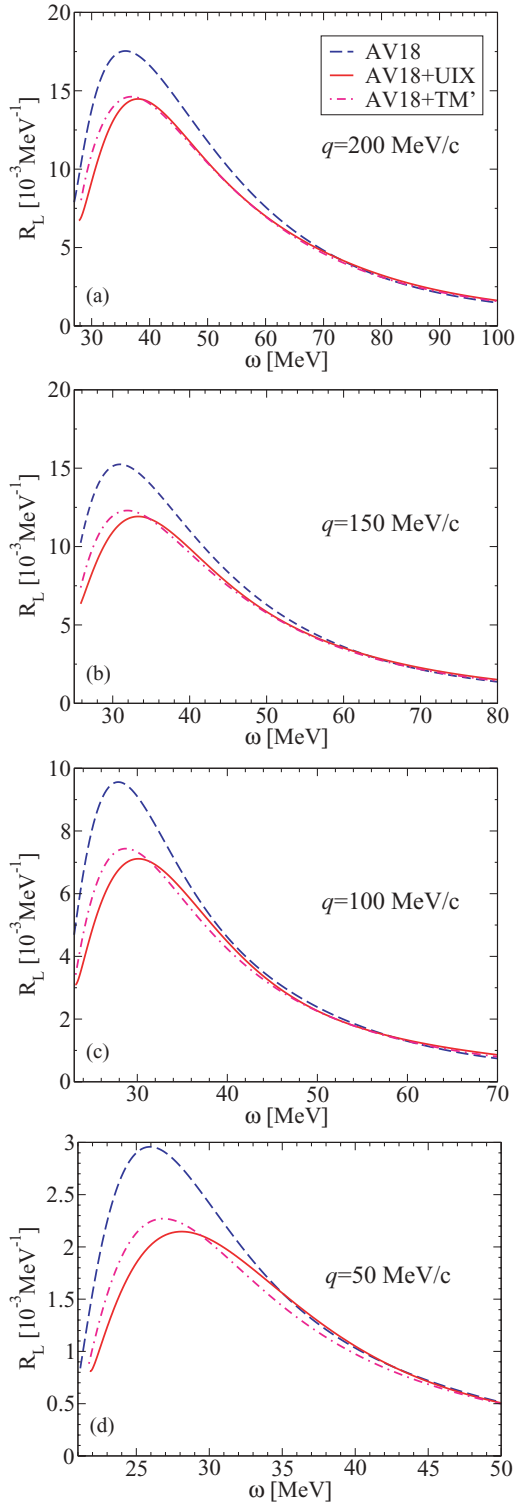

FIG. 2. (Color online) Longitudinal response function for $q = 200$, 150, 100, and 50 MeV/c with the AV18 two-nucleon force only (dashed line) and with the addition of the UIX (solid line) or the TM′ (dashed-dotted line) three-nucleon force.

using the Tucson-Melbourne′ (TM′) [24] three-nucleon force. Whereas the UIX force contains a two-pion exchange and a short-range phenomenological term, with two 3NF parameters fitted on the triton binding energy and on the nuclear matter

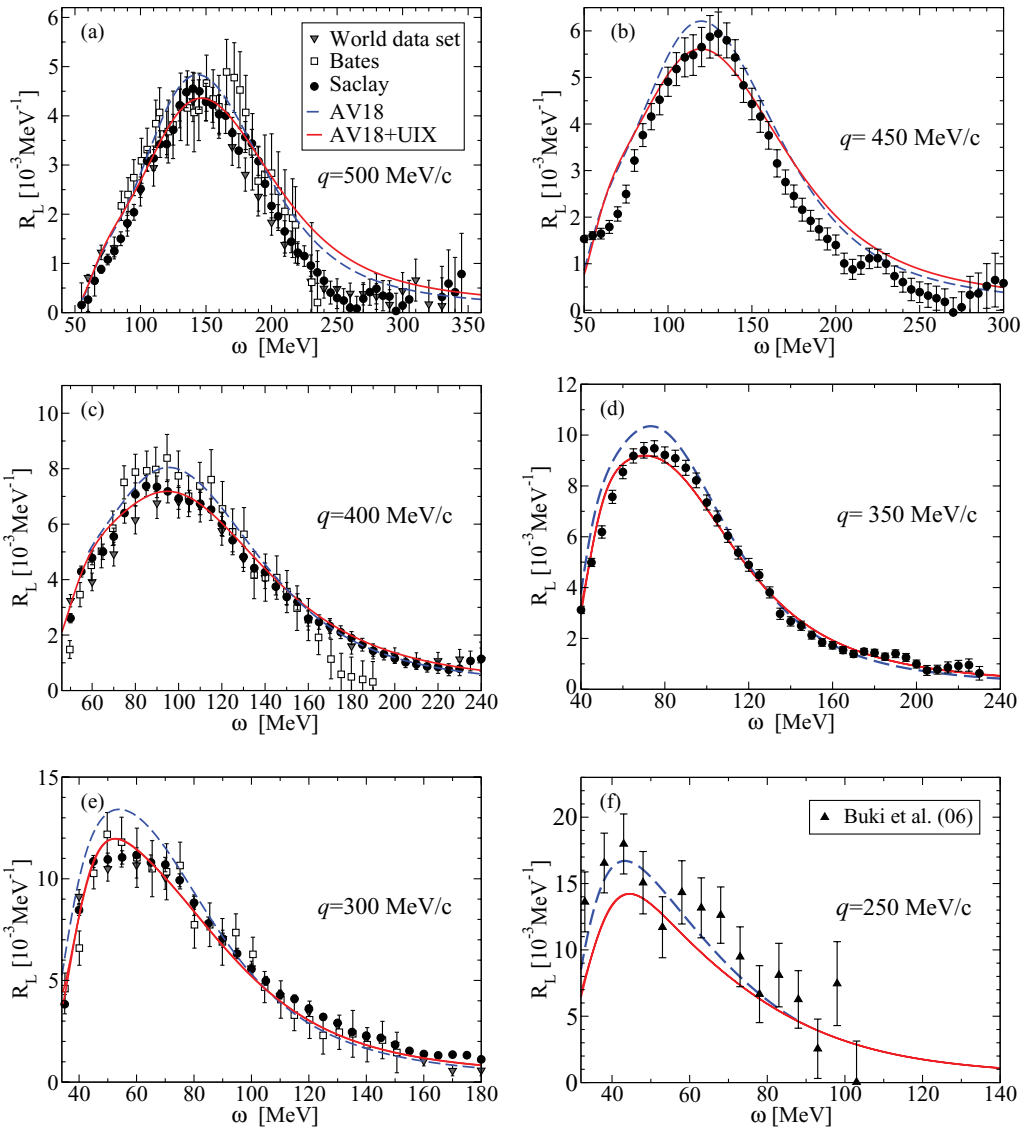

FIG. 3. (Color online) $R_L(\omega, q)$ for $250 \leqslant q \leqslant 500$ MeV/c: calculations with the AV18 (dashed line) and the AV18 + UIX (solid line). Data are from Ref. [28] (squares), Ref. [29] (circles), Ref. [5] (downward-pointing triangles), and Ref. [18] (upward-pointing triangles).

density (in conjunction with the AV18 two-nucleon potential), the TM′ force is not adjusted in this way. It includes two pion exchange terms where the coupling constants are taken from pion-nucleon scattering data consistent with chiral symmetry.

Our results with the TM′ force are obtained using the same model space as for the UIX potential, and the accuracy of the convergence for the LIT is found to be at a percentage level in analogy with that of the UIX as described in Ref. [9]. The cutoff of the TM′ force has been adjusted to describe the triton binding energy when used in conjunction with the AV18 N-N force. With a cutoff $\Lambda = 4.77 m_\pi$, where m_π is the pion mass, we obtain the binding energies 8.47 MeV (^{3}H) and 28.46 MeV (^{4}He). We emphasize that the ^{4}He binding energy is practically the same as that for the AV18 + UIX case (as found in Ref. [25]).

In addition to what was reported in our recent Letter [9], here we also investigate other low q values. Figure 2 shows that the increase in 3NF effects with decreasing q is confirmed. Moreover, it becomes evident that the difference between the results obtained with the two 3NF models also increases with decreasing q. One actually finds that the shift of the peak to higher energies in the case of the UIX generates a difference in R_L of up to about 10% on the low-energy sides of the peaks. This is a very interesting result. It represents the first case of an electromagnetic observable that is considerably dependent on the choice of the 3NF. In the light of these results it would be very interesting to repeat the calculation with effective field theory two- and three-body potentials [26,27]. At the same time it would be highly desirable to obtain precise measurements of R_L at low q. This could serve either to fix the low-energy constants of the effective field theory 3NF or, possibly, to discriminate among different nuclear force models.

Figure 3 gives an overview of the results obtained for higher q, as well as a comparison with existing experimental data. The

3NF results are closer to the data; this is particularly evident at $q = 300$ MeV/c. However, the 3NF effect is generally not as large as for the lower momentum transfers shown in Figs. 2 and 3. In some cases the quenching of the strength due to the 3NF is comparable to the size of the error bars, particularly for the data from Ref. [28]. The largest discrepancies with the data are found at $q = 450$ and 500 MeV/c. Whereas the height of the peak is reproduced well by the result with the 3NF, the width of the experimental peak seems to be somewhat narrower than the theoretical one. However, it must be borne in mind that relativistic effects are not completely negligible at $q \geqslant 450$ MeV/c. They probably play a role similar to that found in the electrodisintegration of three-nucleon systems (see, e.g., Ref. [30]). In the case of $q = 250$ MeV/c the experimental results are not sufficiently precise to draw a conclusion.

IV. MULTIPOLE ANALYSIS

It is interesting to analyze the results of R_L in terms of its multipole contributions. Using Eq. (5) on the right-hand-side of Eq. (8), $\mathcal{L}_L(\sigma, q)$ can be decomposed into a sum of multipole contributions $\mathcal{L}^{J,X}(\sigma, q)$. We have calculated each of them separately, solving the corresponding equations (8). After inversion of the transform we obtain the various multipole responses. By multiplying them by the isoscalar and isovector nucleon form factors, we generate the multipole contributions to the longitudinal response function $R_L^{J,X}(\omega, q)$. Figure 4 shows how the isoscalar and isovector parts of R_L are built up from their multipole contributions at a higher (500 MeV/c) and a lower (100 MeV/c) value of q. As expected, the higher the momentum transfer, the larger the number of multipoles that must be considered to reach convergence. For $q = 500$ MeV/c up to seven multipoles are considered, whereas for $q = 100$ MeV/c, only three multipoles are required for a converged result. Careful readers may notice that the isoscalar response at $q = 100$ MeV/c does not seem to show a convergence in the multipole decomposition. As already mentioned, the isoscalar dipole is negligible (explaining why the curve labeled "0" overlaps the "+1" curve), and a similarly negligible strength is found for the multipoles higher than the quadrupole. Regarding the strength distribution among the multipoles two facts are evident: (i) At higher q the strength is almost equally distributed among the first isovector multipoles, whereas in the isoscalar channel the quadrupole makes the largest contribution, and (ii) at low q, as expected, the response is dominated by the isovector dipole contribution. Whereas the isoscalar dipole is completely negligible, the isoscalar quadrupole contributes a few percent. These facts are also illustrated in Fig. 5, where the total strength of the various multipoles, defined as

$$m^{J,X} = \int_{\omega_{\rm th}}^{\infty} d\omega R_L^{J,X}(\omega, q), \tag{14}$$

is shown for $q = 100$, 300, and 500 MeV/c. At $q = 100$ MeV/c the $J = 1$ and $J = 3$ multipoles of the isoscalar response are tiny. The $J > 3$ multipoles are neglected in Figs. 1, 2, and 4 for the $q \leqslant 100$ MeV/c kinematics. We must point out that the total strengths presented in Fig. 5 do not contain the nucleon form factors. The strengths can be obtained by integrating in energy (up to infinity) the inversion of $\mathcal{L}^{J,X}(\sigma, q)$ (non-energy-weighted sum rule) or just by taking

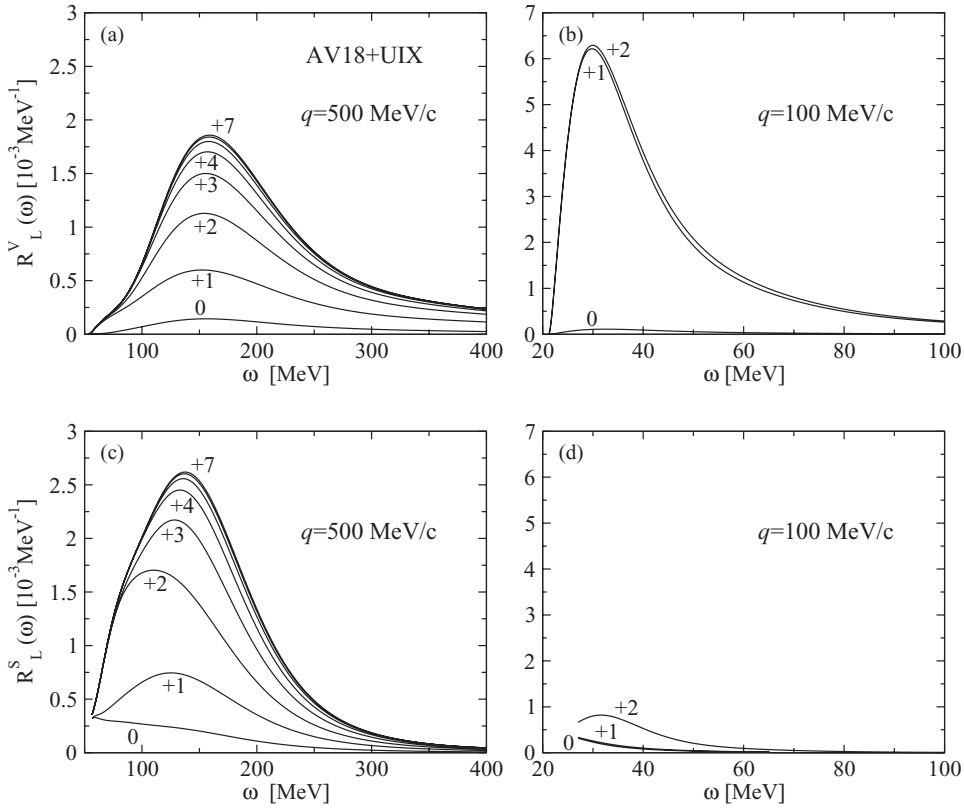

FIG. 4. Response functions of the lowest isovector (upper panel) and isoscalar (lower panel) Coulomb multipoles, starting with the monopole and consecutively adding higher multipoles up to $J_{\rm max} = 7$ for $q = 500$ MeV/c (left) and $J_{\rm max} = 2$ for $q = 100$ MeV/c (right) in the case of the AV18 + UIX potential.

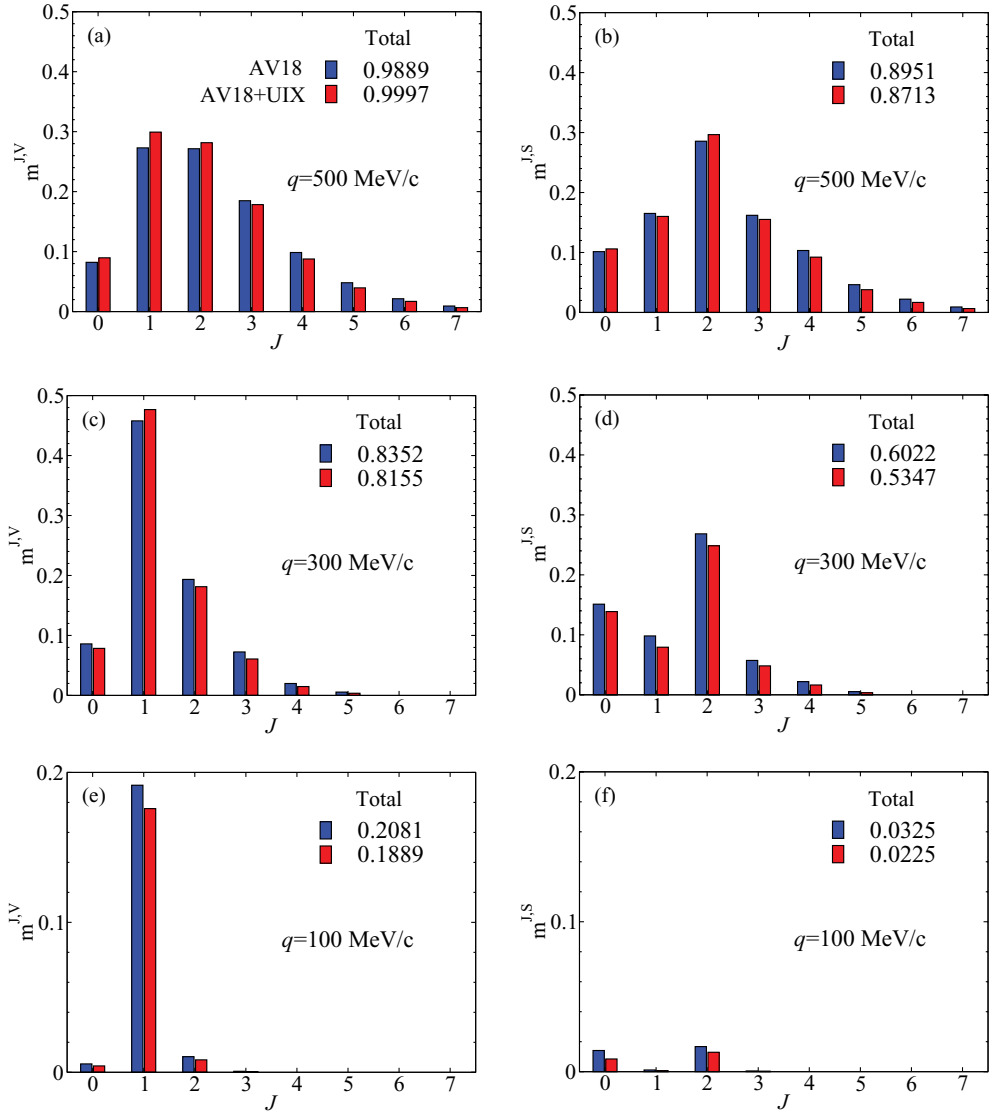

FIG. 5. (Color online) Isovector (left panels) and isoscalar (right panels) multipole strength distribution of R_L at $q = 500$, 300, and 100 MeV/c in the case of the AV18 and AV18 + UIX potentials. The sum of all isovector and all isoscalar multipoles for the two potentials is also shown in the legend.

the norm of the right-hand-side of Eq. (8) for each multipole, that is, the norm of $\hat{C}^{J,X}(q)|\Psi_0\rangle$.

In Fig. 5, 3NF effects are also illustrated. The three q values shown give an idea of the evolution of the effect from the short-range to the long-range regime. At the highest q value the three strongest contributions are given by the isovector dipole and the isoscalar and isovector quadrupoles. They are enhanced by the 3NF, whereas all other multipoles are decreased, resulting in a net small quenching effect. At $q = 300$ MeV/c there is a kind of transition situation where only the still dominating isovector dipole strength is increased by the 3NF, whereas all other multipoles are quenched. At $q = 100$ MeV/c the strength of all multipoles is decreased by the 3NF, resulting in an overall sizable quenching effect.

In Fig. 6, the effect just described shows up more clearly in the energy distribution of the dominant multipole contributions (isovector dipole and isoscalar quadrupole) at $q = 500$ and 100 MeV/c. In particular, at $q = 500$ MeV/c the increase in the strength due to the 3NF in the isovector dipole channel is found mainly in the high-energy tail, whereas in the isoscalar quadrupole the increase is found around the peak. At $q = 100$ MeV/c the situation is different in that the quenching of the strength due to the 3NF is concentrated in the peak region, for both multipoles. The net result of this mechanism is the increase in the 3NF quenching effect with decreasing q that is evident in Fig. 2.

Here we would like to comment on the fact that the large contribution of the 3NF at low q seems at variance with the smaller contribution to the photoabsorption cross section [22], also dominated by the isovector dipole. The reason is twofold. It has to do, on the one hand, with the correct use of the Siegert theorem and, on the other hand, with the common procedure of letting theoretical cross sections start from the experimental

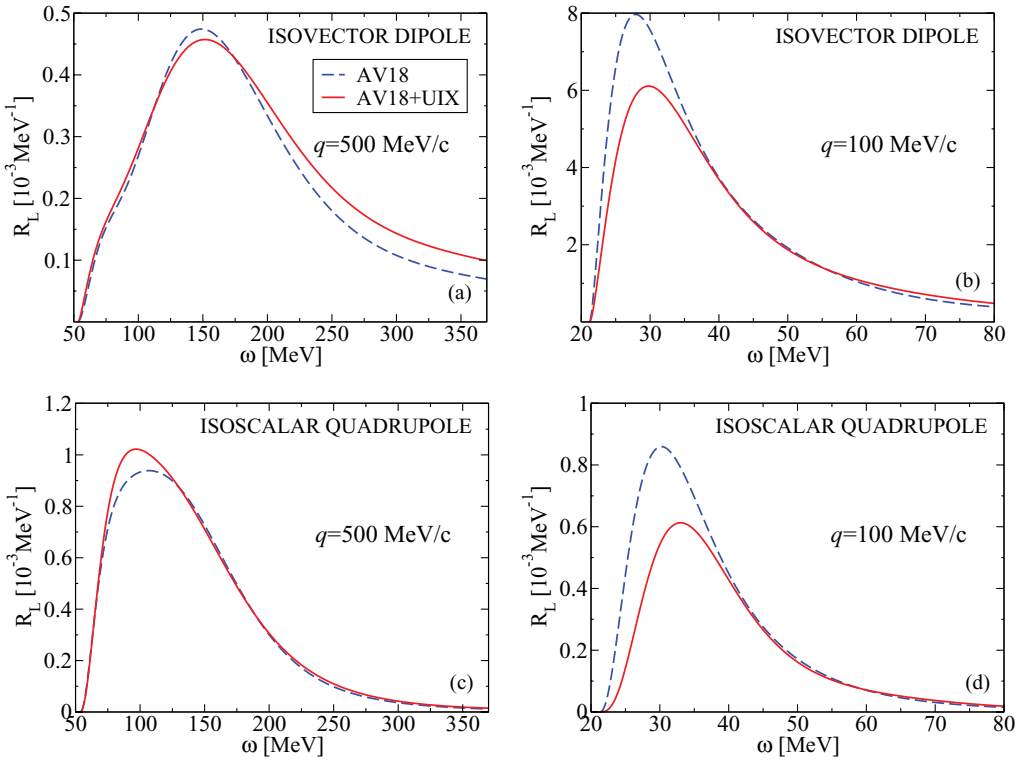

FIG. 6. (Color online) Response functions of the isovector dipole and isoscalar quadrupole for $q = 500$ MeV/c and $q = 100$ MeV/c with the AV18 (dashed line) and AV18 + UIX (solid line) potentials.

threshold, also when the binding energies do not reproduce the experimental values. A detailed explanation is in order here. Because of charge conservation the relation (Siegert theorem) between the charge dipole matrix element ($C^{1,V}$) considered here and the electric dipole matrix element ($E1$) considered in the photon case implies the factor $(E_n - E_0)$ (see also Ref. [31]). The binding energy $(-E_0)$ of ^{4}He, however, is about 15% lower for the AV18 than it is for the AV18 + UIX. The following consequences occur. In the AV18 + UIX case in Ref. [22] the result of the squared matrix element is multiplied by $[E_n - E_0(\mathrm{AV18 + UIX})]$, which is equal to ω_γ, whereas in the AV18 case multiplication by $[E_n - E_0(\mathrm{AV18})]$ implies a smaller multiplicative factor. Therefore the quenching three-body effect is smaller. Only thereafter is the AV18 ^{4}He total photoabsorption cross section shifted to the experimental threshold.

The procedure of shifting the theoretical cross sections to the experimental threshold might seem questionable, but without such a shift all 3NF effects would be greatly amplified in the photoabsorption cross section and even in the present response function results. However, in this case they are, in a way, "trivial binding effects."

V. INTEGRAL PROPERTIES OF R_L

There are many examples in different fields of physics where a certain observable cannot be accessed, but only some of its integral properties. Sum rules (nth moments of the energy distribution) [32] are well-known examples. They contain some often very useful, although limited, information about the observable. The more sum rules one knows, the larger the amount of information at one's disposal. Integral transforms can also be viewed as a special form of sum rules. Whereas sum rules map an energy-dependent observable into a set of n discrete values, integral transforms map the same observable into a continuous set of parameters.

Reconstructing the searched observable from its integral properties can be very difficult, as very often only a limited number of moments are known or, in the case of integral transforms, the result of the mapping does not resemble the observable of interest at all. This is not the case for the LIT. An example is illustrated in Fig. 7(a), where $R_L(\omega, q = 300\,\mathrm{MeV}/c)$ for the AV18 + UIX potential [as in Fig. 3(e)] is compared with the corresponding LIT, $\mathcal{L}_L(\sigma, q)$, calculated using a typical value of σ_I (20 MeV). The similarity between the shape of the response function and that of its integral transform is apparent. This similarity is due to the fact that the Lorentz kernel is a representation of the δ function. It is this property that makes the inversion of the integral transform [34] reliable and sufficiently accurate for the Lorentz kernel. This situation must be confronted with the Laplace transform. The Laplace transform of R_L, called the Euclidean response, is given by [33]

$$\mathcal{E}(\tau, q) = \int_{\omega_{th}}^{\infty} d\omega \, \exp\left[-\tau\left(\omega - \frac{q^2}{2m}\right)\right] \frac{R_L(\omega, q)}{Z\left|G_E^p(Q^2)\right|^2}. \tag{15}$$

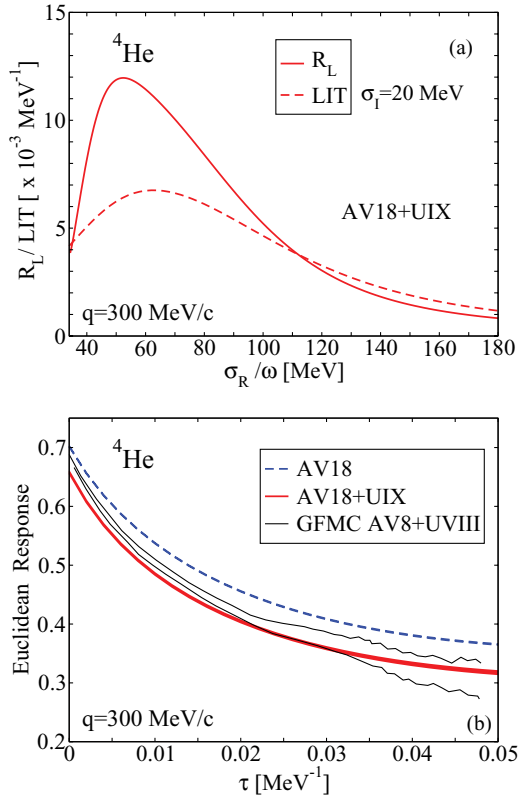

FIG. 7. (Color online) (a) Longitudinal response function R_L (solid line) at $q = 300$ MeV/c with its Lorentz integral transform (LIT; dashed line) for the AV18 + UIX potential. The LIT has been multiplied by σ_I/π to normalize the integral kernel with respect to Eq. (7). (b) Euclidean longitudinal response for the same momentum transfer: Comparison of the GFMC calculation [33] for the AV8 + UVIII potential (band between thin lines) and the result of this work with the AV18 (dashed line) and the AV18 + UIX (solid line).

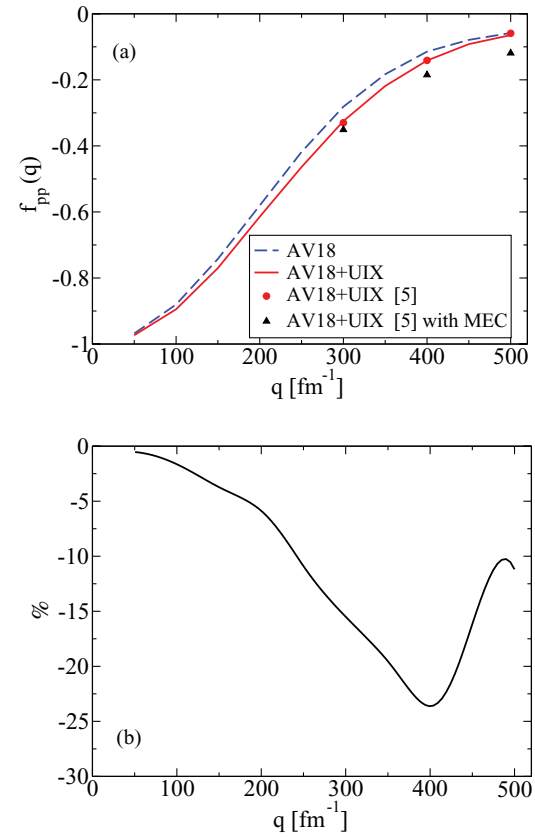

FIG. 8. (Color online) (a) $f_{pp}(q)$ in the CSR [Eq. (16)] with AV18 (dashed) and AV18 + UIX (solid line) potentials. Circles show results from Ref. [5] with the one-body density operator in Eq. (3), and triangles are the results from Ref. [5] with the two-body density operator. (b) Percentage difference between the curves in (a).

Figure 7(b) shows that $\mathcal{E}(\tau, q)$ exhibits a completely different form than $R_L(\omega, q)$ does. It is interesting that, even in τ space, the Euclidean response obtained using only the two-body potential gives a result much different from that obtained with the 3NF included. However, what is not evident from $\mathcal{E}(\tau, q)$ is in which energy region the contribution of the 3NF is important.

Figure 7(b) also shows a comparison of our results with those from Ref. [33] obtained with the Monte Carlo method. The comparison is of interest, even if the potentials used in the two cases are slightly different. (In Ref. [33] the older versions of the Argonne and Urbana, AV8 and UVIII, were used.) At τ larger than 0.02, our result with the AV18 + UIX lies within the error band of the Monte Carlo numerical noise. At smaller τ, in particular, at $\tau = 0$, Fig. 7(b) shows a discrepancy between the present $\mathcal{E}(\tau, q)$ and that in Ref. [33]. This is certainly caused by the different potentials used. The $\mathcal{E}(0, q)$ value corresponds to the zeroth moment of $R_L(\omega, q)$. This is a classical integral property of $R_L(\omega, q)$ that has been much discussed in the literature under the name of Coulomb sum rule (CSR). (For a review see Refs. [32] and [35].) The sum rule consists in connecting the integral of the inelastic longitudinal response to the number of protons and to the Fourier transform of the proton-proton correlation function $\rho_{pp}(s)$, that is, the probability of finding two protons at a distance s. In fact for the charge density operator in Eq. (3) (and neglecting the neutron charge form factor), one has

$$\mathrm{CSR}(q) \equiv \int_{\omega_{\rm th}}^{\infty} d\omega \frac{R_L(\omega, q)}{\left|G_E^p(Q^2)\right|^2} = Z + Z(Z-1) f_{pp}(q) - Z^2 |F(q)|^2, \qquad (16)$$

where $f_{pp}(q)$ is the Fourier transform of $\rho_{pp}(s)$ and $F(q)$ is the nuclear elastic form factor. The main feature of interest in the CSR(q) to date has been its very simple, model-independent high-q limit, that is, the number of protons. Deviations of the "experimental" CSR from Z have been ascribed to relativistic corrections, exchange current contributions, in-medium nucleon form factors, and so on. Instead we concentrate on $f_{pp}(q)$, because it contains interesting physical information about the proton-proton correlation function. [Another interesting sum rule concerning the second moment $\langle s^2 \rangle$ of $\rho_{pp}(s)$, i.e., the low-q limit of $f_{pp}(q)$, was considered in Ref. [36], where it was found that $\langle s^2 \rangle = 5.67$ fm^2 for AV18 + UIX.]

In Fig. 8, $f_{pp}(q)$ is shown in comparison with the results from Ref. [5] obtained with the same potential, including,

TABLE I. Theoretical CSR for low q with the AV18 + UIX potential in comparison with $I_\gamma^{\rm th} = \int_{\omega_{\rm th}}^{\omega=q} d\omega R_L^{\rm exp}(q,\omega)/|G_E^p(Q^2)|^2$. The percentage contribution of the timelike response is also listed.

q (MeV/c)	CSR(q)	$I_\gamma^{\rm th}$	% timelike
50	3.88	3.86	0.5
100	3.57	3.55	0.6
150	3.17	3.14	0.9
200	2.79	2.74	1.5

in addition, the lowest order relativistic corrections as well as exchange operators, neglected here. We can make the following observations. (i) The perfect agreement of the two results when the operator in Eq. (3) is used shows the high accuracy of the two calculations. (ii) The contributions of exchange currents become negligible below $q = 300$ MeV. This means that at low q physical interpretation of $f_{pp}(q)$ as the Fourier transform of $\rho_{pp}(s)$ is safe. Therefore, in principle, the comparison of theory versus experiment would allow microscopic study of the largely unknown long-range correlations. (iii) As shown in Fig. 8(b) the effect of the 3NF on $f_{pp}(q)$ is up to 15% in the "safe" region below $q =$ 300 MeV/c. This gives an idea of the required experimental accuracy.

Unfortunately, obtaining the "experimental" CSR(q) [as well as $\mathcal{E}(0,q)$] is a nontrivial task, owing to the necessity of extrapolating data up to infinite energies, even crossing the photon point, where (e,e') measurements do not have access. Different extrapolation functions have been proposed. They were also used recently in Ref. [18]. Our results can help to determine these tail contributions. They can in fact be obtained by subtracting from CSR(q) the experimental sum of the data up to the last measured point at $\omega_{\rm max}$. From the Saclay data [29] at $q = 300$ and 350 MeV/c we estimated this high-energy contribution to be about 7% of the CSR. The effect becomes twice as large for higher q values. However, although this procedure would be safe enough at low q, at high q this estimate could be inaccurate because of the neglect of relativistic effects, two-body operators, and the role of the neutron form factor. In general it would be desirable for the tail contribution not to overcome the 3NF effect. Therefore accurate data should be taken as far in energy as possible. Of course they cannot overcome the photon point; therefore it is of interest to calculate the contribution of the tail beyond it. Table I reports that for q values up to 200 MeV/c the contribution of the timelike region remains very low, reaching at most 1.5%.

The present discussion, besides being interesting from a purely theoretical point of view, may help to access information about the proton-proton correlation function from experimental data.

VI. CONCLUSIONS

In this paper we have analyzed 3NF effects on the electron scattering longitudinal response function at several kinematics. The most interesting results regard momentum transfers between 50 and 250 MeV/c. Large effects of 3NFs are found for two three-body potentials (Urbana IX and Tucson-Melbourne′), starting from an AV18 two-body potential. We also observe that the 3NF effects differ by nonnegligible amounts for the two three-body force models. Because the difference between the two results increases with decreasing momentum transfer, it can be ascribed to the rather different long-range correlations generated by the two forces. This observation suggests that discriminating between phenomenological and effective field theory potentials might also be possible, if precise experimental data were available at these kinematics.

Three-body force effects have been analyzed separately in the various multipoles contributing to the response. Below $q = 300$ MeV/c a cooperative quenching effect was found in all multipoles.

Integral properties of the longitudinal response function have also been addressed. In particular, the possibility of extracting information about the long-range behavior of the proton-proton correlation function has been discussed. In relation to this it has been emphasized how the present results can be used in determining the energy tail contributions to the CSR.

In general it has been emphasized that, unlike the search for short-range correlations, the study of long-range ones is not affected by complications owing to relativistic and two-body contributions. Therefore a Rosenbluth separation of the inclusive electron scattering cross section of ^{4}He at momentum transfer $q \leqslant 200$ MeV/c would be of great value for more accurate determination of three-body forces and, in general, of the long-range dynamics of this system.

ACKNOWLEDGMENTS

We would like to thank Alexandr Buki for providing us with information about the data in Ref. [18]. Numerical calculations were partially performed at CINECA (Bologna). This work was supported in part by the Natural Sciences and Engineering Research Council (NSERC) and by the National Research Council of Canada. The work of N. Barnea was supported by Israel Science Foundation Grant No. 361/05.

[1] S. C. Pieper, K. Varga, and R. B. Wiringa, Phys. Rev. C **66**, 044310 (2002), and references therein.

[2] P. Navràtil, V. G. Gueorguiev, J. P. Vary, W. E. Ormand, and A. Nogga, Phys. Rev. Lett. **99**, 042501 (2007), and references therein.

[3] A. Kievsky, S. Rosati, M. Viviani, L. E. Marcucci, and L. Girlanda, J. Phys. G **35**, 063101 (2008), and references therein.

[4] A. Deltuva, A. C. Fonseca, and S. K. Bogner, Phys. Rev. C **77**, 024002 (2008).

[5] J. Carlson, J. Jourdan, R. Schiavilla, and I. Sick, Phys. Rev. C **65**, 024002 (2002).
[6] V. D. Efros, W. Leidemann, and G. Orlandini, Phys. Lett. **B338**, 130 (1994).
[7] V. D. Efros, W. Leidemann, G. Orlandini, and N. Barnea, J. Phys. G Nucl. Part. Phys. **34**, R459 (2007).
[8] T.-S. Park *et al.*, Phys. Rev. C **67**, 055206 (2003).
[9] S. Bacca, N. Barnea, W. Leidemann, and G. Orlandini, Phys. Rev. Lett. **102**, 162501 (2009).
[10] J. M. Eisenberg and W. Greiner, *Excitation Mechanisms of the Nucleus* (North-Holland, Amsterdam, 1970).
[11] N. Barnea and A. Novoselsky, Ann. Phys. (NY) **256**, 192 (1997).
[12] N. Barnea, W. Leidemann, and G. Orlandini, Phys. Rev. C **61**, 054001 (2000); Nucl. Phys. **A693**, 565 (2001).
[13] N. Barnea, V. D. Efros, W. Leidemann, and G. Orlandini, Few-Body Syst. **35**, 155 (2004).
[14] V. D. Efros, W. Leidemann, and G. Orlandini, Few-Body Syst. **26**, 251 (1999).
[15] D. Andreasi, W. Leidemann, C. Reiß, and M. Schwamb, Eur. Phys. J. A **24**, 361 (2005).
[16] N. Barnea, V. D. Efros, W. Leidemann, and G. Orlandini, arXiv:0906.5421.
[17] S. Galster *et al.*, Nucl. Phys. **B32**, 221 (1971).
[18] A. Yu. Buki, I. S. Timchenko, N. G. Shevchenko, and I. A. Nenko, Phys. Lett. **B641**, 156 (2006).
[19] R. B. Wiringa, V. G. J. Stoks, and R. Schiavilla, Phys. Rev. C **51**, 38 (1995).
[20] B. S. Pudliner, V. R. Pandharipande, J. Carlson, S. C. Pieper, and R. B. Wiringa, Phys. Rev. C **56**, 1720 (1997).
[21] R. A. Malfliet and J. A. Tjon, Nucl. Phys. **A127**, 161 (1969).
[22] D. Gazit, S. Bacca, N. Barnea, W. Leidemann, and G. Orlandini, Phys. Rev. Lett. **96**, 112301 (2006).
[23] Th. Walcher, Phys. Lett. **B31**, 442 (1970); Z. Phys. **237**, 368 (1970).
[24] S. A. Coon and H. K. Hahn, Few-Body Syst. **30**, 131 (2001).
[25] A. Nogga, H. Kamada, W. Glöckle, and B. R. Barrett, Phys. Rev. C **65**, 054003 (2002).
[26] D. R. Entem and R. Machleidt, Phys. Rev. C **68**, 041001(R) (2003).
[27] E. Epelbaum, W. Glöckle, and U. G. Meißner, Nucl. Phys. **A747**, 362 (2005).
[28] S. A. Dytman *et al.*, Phys. Rev. C **38**, 800 (1988).
[29] A. Zghiche *et al.*, Nucl. Phys. **A572**, 513 (1994).
[30] V. D. Efros, W. Leidemann, G. Orlandini, and E. L. Tomusiak, Phys. Rev. C **72**, 011002(R) (2005).
[31] S. Bacca, H. Arenhövel, N. Barnea, W. Leidemann, and G. Orlandini, Phys. Rev. C **76**, 014003 (2007).
[32] G. Orlandini and M. Traini, Rep. Prog. Phys. **54**, 257 (1991).
[33] J. Carlson and R. Schiavilla, Phys. Rev. C **49**, R2880 (1994).
[34] A. N. Tikhonov and V. Y. Arsenin, *Solutions of Ill-Posed Problems* (Winston, Washington, DC, 1977).
[35] O. Benhar, D. Day, and I. Sick, Rev. Mod. Phys. **80**, 189 (2008).
[36] D. Gazit, N. Barnea, S. Bacca, W. Leidemann, and G. Orlandini, Phys. Rev. C **74**, 061001(R) (2006).